Cell Death and Differentiation (2016) 23, 76–88
© 2016 Macmillan Publishers Limited All rights reserved 1350-9047/16
www.nature.com/cdd

Characterization of RIPK3-mediated phosphorylation of the activation loop of MLKL during necroptosis

DA Rodriguez[1,5], R Weinlich[1,5,6], S Brown[1], C Guy[1], P Fitzgerald[1], CP Dillon[1], A Oberst[2], G Quarato[1], J Low[3], JG Cripps[4], T Chen[3] and DR Green*[,1]

Mixed lineage kinase domain-like pseudokinase (MLKL) mediates necroptosis by translocating to the plasma membrane and inducing its rupture. The activation of MLKL occurs in a multimolecular complex (the 'necrosome'), which is comprised of MLKL, receptor-interacting serine/threonine kinase (RIPK)-3 (RIPK3) and, in some cases, RIPK1. Within this complex, RIPK3 phosphorylates the activation loop of MLKL, promoting conformational changes and allowing the formation of MLKL oligomers, which migrate to the plasma membrane. Previous studies suggested that RIPK3 could phosphorylate the murine MLKL activation loop at Ser345, Ser347 and Thr349. Moreover, substitution of the Ser345 for an aspartic acid creates a constitutively active MLKL, independent of RIPK3 function. Here we examine the role of each of these residues and found that the phosphorylation of Ser345 is critical for RIPK3-mediated necroptosis, Ser347 has a minor accessory role and Thr349 seems to be irrelevant. We generated a specific monoclonal antibody to detect phospho-Ser345 in murine cells. Using this antibody, a series of MLKL mutants and a novel RIPK3 inhibitor, we demonstrate that the phosphorylation of Ser345 is not required for the interaction between RIPK3 and MLKL in the necrosome, but is essential for MLKL translocation, accumulation in the plasma membrane, and consequent necroptosis.
Cell Death and Differentiation (2016) **23,** 76–88; doi:10.1038/cdd.2015.70; published online 29 May 2015

Regulated necrotic cell death, or 'necroptosis,' is mediated by the interaction of activated receptor-interacting kinase-3 (RIPK3) and mixed lineage kinase like (MLKL).[1–3] The function of RIPK3 to promote necroptosis can be induced by the activity of receptor-interacting protein kinase-1 (RIPK1),[4] and is antagonized by the proteolytic activity of a complex formed by RIPK1, FADD, caspase-8 and c-FLIP$_L$.[5–10] Inactive RIPK1 functions to inhibit RIPK3 activation, even under conditions in which RIPK3 is activated independently of RIPK1.[11–13] These complex interactions help to account for the lethal effects of ablating FADD, caspase-8 or RIPK1.[14]

MLKL is a substrate for RIPK3 kinase activity[1–3] and appears to execute the process of necroptosis by targeting the plasma membrane.[15–17] The phosphorylation of MLKL by RIPK3 has been proposed to promote necroptosis by inducing essential changes in the 'latch' of this pseudokinase, allowing the formation of oligomers, migration to plasma membrane[15–18] and binding to phosphatidylinositol lipids to directly disrupt membrane integrity.[16,19] Structurally, murine MLKL is composed of a pseudokinase domain (C-terminal region) and a four-helical bundle domain (4HBD) located in the N-terminal region.[3,20] The 4HBD domain is sufficient to oligomerize, bind to phosphatidylinositol lipids and trigger cell death.[16,19] However, the activation of full-length MLKL requires phosphorylation of residues in the activation loop in the pseudokinase domain. The residues Ser345, Ser347 and Thr349 within the murine MLKL activation loop are RIPK3 phosphorylation sites,[3] corresponding to Thr357 and Ser358 in human MLKL.[16] Upon RIPK3 phosphorylation, human MLKL shifts from its monomeric state to an active oligomeric state.[16]

The residue Gln343 in the murine α-helix (residues Leu339 to Ser347) forms a hydrogen bond with Lys219 and the Ser345 and disruption of this coordinated state by phosphorylation of Ser345 has been proposed to destabilize the monomeric structure, promoting a conformational change in MLKL to an active state.[3,21] This hypothesis was supported by the specific mutations K219M, Q343A or S345D; all of which led to a form of MLKL form that promoted necroptosis independently of RIPK3.[3,16]

In this study, we examine serine and threonine residues within the activation loop of MLKL for their roles in necroptosis. We have developed an antibody anti-phospho-Ser345 and explore its use as a marker for necroptosis in murine cell systems. Using this antibody, together with described and

[1]Department of Immunology, St Jude Children's Research Hospital, Memphis, TN 38105, USA; [2]Department of Immunology, University of Washington, Seattle, WA 98109, USA; [3]Department Chemical Biology & Therapeutics, St Jude Children's Research Hospital, Memphis, TN 38105, USA and [4]Institute for Cellular Therapeutics, University of Louisville, Louisville, KY 40202, USA

*Corresponding author: DR Green, Department of Immunology, St Jude Children's Research Hospital, MS 351, Room E7050, 262 Danny Thomas Place, Memphis, TN 38105, USA. Tel: +1 (901) 595 3488; Fax: +1 (901) 595 5766; E-mail: douglas.green@stjude.org

[5]These authors contributed equally to this work.

[6]Current address: Hospital Israelita Albert Einstein, São Paulo 05652-900, Brazil.

Abbreviations: 4HBD, four-helical bundle domain; AP 20187, homodimerization drug; BMH, bis(maleimido)hexane; CHX, Cycloheximide; DOX, Doxycycline; FADD, fas-associating death domain-containing protein; ELISA, Enzyme-Linked ImmunoSorbent Assay; IFNβ, Interferon β; LPS, lipopolysaccharide; MEF, murine embryonic fibroblast; MLKL, mixed lineage kinase like; Nec-1, necrostatin-1; Poly I:C, Polyinosinic:polycytidylic acid; qVD, Q-VD-OPh (Quinolyl-Val-Asp-OPh); RHIM, RIP homotypic interaction motif; RIPK1, receptor-interacting protein kinase-1; RIPK3, receptor-interacting protein kinase-3; TBST, Tris-buffered saline containing Tween-20; TNF, tumor necrosis factor; zVAD, Z-val-ala-asp-(O-methylated)-fluoromethylketone.

Received 16.3.15; revised 28.4.15; accepted 28.4.15; Edited by G Melino; published online 29.5.15

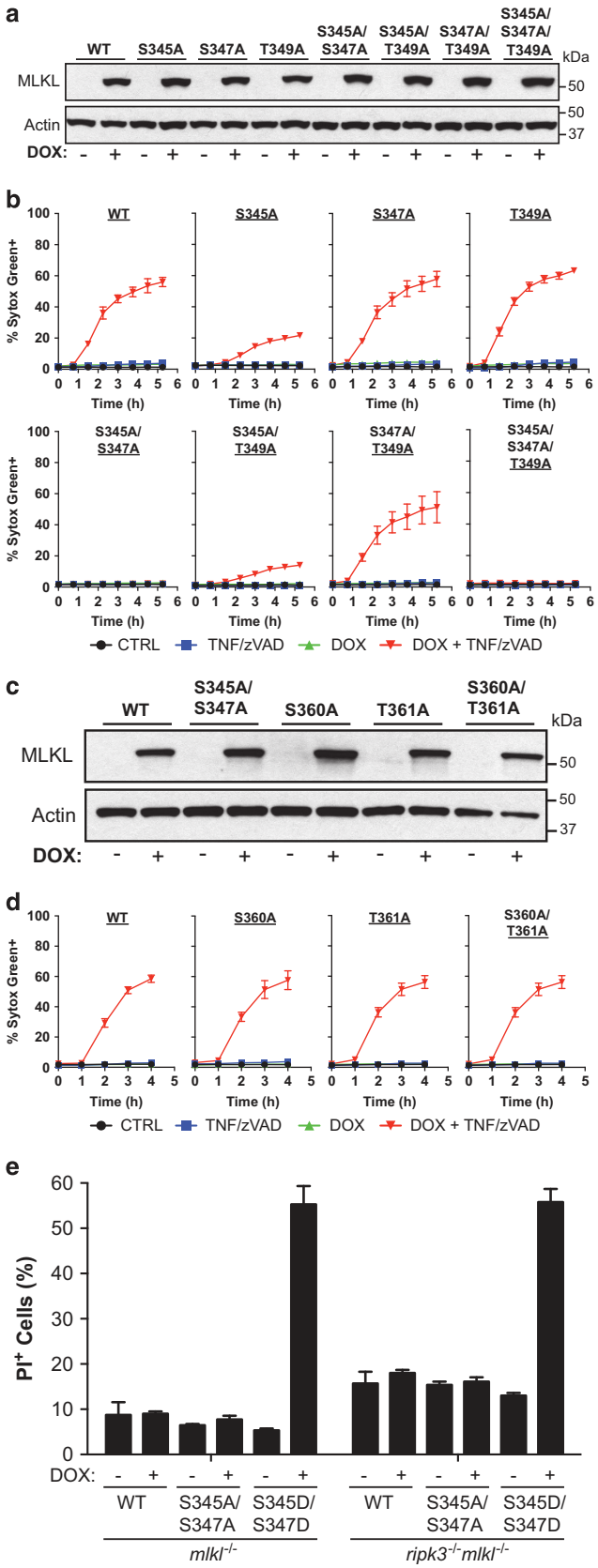

novel inhibitors of RIPK3, we more fully explore the role of modifications in the active loop of MLKL during the process of necroptosis.

Results

Phosphorylation of Ser345 is a key event in the activation of MLKL by RIPK3. During necroptosis, RIPK3 phosphorylates MLKL on different residues, including Ser345, Ser347 and Thr349,[3] thus activating its effector function.[2,16] MLKL in which one, two or all three of these residues were replaced by alanines was expressed under a doxycycline (DOX)-controlled promoter in immortalized *mlkl*$^{-/-}$ murine embryonic fibroblast (MEF).[11] These constructs were expressed at similar levels upon DOX treatment (Figure 1a) and, as expected, cells expressing WT MLKL died upon stimulation with tumor necrosis factor (TNF) plus zVAD (Z-val-ala-asp-(O-methylated)-fluoromethylketone) only when pretreated with DOX (Figure 1b).

Cells expressing the single mutant S345A showed resistance to TNF plus zVAD-induced necroptosis, whereas cells harboring either the single mutants S347A and T349A or the double mutant S347A, T349A behaved similarly to the WT (Figure 1b). The double mutant S345A, S347A was completely resistant, whereas the double mutant S345A, T349A did not increase the level of resistance beyond that of S345A (Figure 1b). The triple mutant was as insensitive to TNF plus zVAD-induced death as the double mutant S345A, S347A (Figure 1b).

Two additional potential phospho-targets (www.phosphosite.org), Ser360 and Thr361, were assessed. DOX treatment of stably transduced *mlkl*$^{-/-}$ MEF induced similar levels of expression among the WT, single (S360A or T361A) and double MLKL mutants (Figure 1c). None of the mutants displayed reduced necroptosis upon TNF plus zVAD treatment (Figure 1d).

To investigate whether Ser345 and Ser347 are not only critical but also sufficient for MLKL activation, both of these residues were replaced by aspartate (S345D, S347D) to create a phospho-mimic MLKL. Expression of this mutant induced cell death even in the absence of TNF plus zVAD stimulation (Figure 1e). Similar results were observed upon expression in *ripk3*$^{-/-}$*mlkl*$^{-/-}$ MEF (Figure 1e).

Murine MLKL is acetylated at Lys77.[22] As acetylation can alter the state of activation of a protein as well as its ability to

Figure 1 Combined mutations in the activation loop of MLKL abrogate RIPK3-mediated activation upon TNF plus zVAD stimulation. (**a** and **b**) *Mlkl*$^{-/-}$ MEF expressing DOX-inducible WT, single (S345A, S347A and T349A), double (S345A/S347A, S345A/T349A and S347A/T349A) or triple (S345A/S347A/T349A) MLKL-FLAG (C-Term) were stimulated with 1 μg/ml DOX for 8 h. (**c** and **d**) *Mlkl*$^{-/-}$ MEF expressing DOX-inducible WT, single (S360A and T361A) or double (S345A/S347A and S360A/T361A) MLKL-FLAG (C-Term) were stimulated with 1 μg/ml DOX for 8 h. (**a** and **c**) Western blots for MLKL expression. Actin was used as loading control. (**b** and **d**) After DOX treatment, cells were stimulated or not with 10 ng/ml TNF and 25 μM zVAD. Cell death was monitored by Sytox Green uptake using an Incucyte Kinetic Live Cell Imager. Data are representative of three independent experiments. Error bars, s.d. (**e**) *Mlkl*$^{-/-}$ or *ripk3*$^{-/-}$*mlkl*$^{-/-}$ MEF expressing WT, S345A/S347A or S345D/S347D MLKL-FLAG (C-Term) were stimulated with 1 μg/ml DOX and cell death was assessed by propidium iodide uptake via flow cytometry (PI^{+} cells (%)) after 16 h. Data are representative of two independent experiments. Error bars, s.d.

interact with other proteins,[23] Lys77 was replaced with either alanine (K77A) or arginine (K77R). DOX-induced expression of these mutants was not toxic to *mlkl*$^{-/-}$ MEF and TNF plus zVAD stimulation induced similar necroptosis as that observed for WT MLKL (Supplementary Figure 1).

Therefore, Ser345 is a key residue for TNF plus zVAD-induced RIPK3-mediated activation of MLKL. Phosphorylation of residues Thr349, Ser360 and Thr361 or acetylation of Lys77 did not affect necroptosis.

Detection of active pSer345-MLKL. As MLKL Ser345 is a key residue for RIPK3-mediated activation of MLKL, we generated a monoclonal antibody specific for MLKL phosphorylated at this site. *Mlkl*$^{-/-}$ mice were immunized with a phosphorylated Ser345 (pS345) peptide from the murine MLKL sequence. Primary screening resulted in polyclonal antisera that recognized the pS345 peptide but not control peptides (Supplementary Figure 2a). A hybridoma clone (pS345-7C6.1) showing specificity for pS345-MLKL was selected (Figure 2a). The antibody was then tested in cell lysates from *mlkl*$^{-/-}$ MEF expressing DOX-controlled WT MLKL-FLAG (C-Term) under conditions of necroptosis. As expected, samples that did not express MLKL or that did express MLKL but without any necroptotic stimulus were negative for pS345-MLKL (pMLKL). However, upon TNF plus zVAD treatment, pMLKL was detected after 2 h of stimulation (Figure 2b). At this time point, 25–30% of cells displayed cell death (as observed in Figures 1b and d).

Mlkl$^{-/-}$ MEF expressing FLAG-MLKL (N-Term) do not die upon stimulation of necroptosis, although MLKL can still be found in the active necrosome.[11] In these cells, pretreatment with DOX followed by TNF plus zVAD stimulation resulted in pMLKL (Supplementary Figure 2b). The same pattern was also observed via ELISA (Supplementary Figure 2c).

To evaluate the specificity of the pS345-7C6.1 antibody for pSer345 detection in cells, *mlkl*$^{-/-}$ MEF cells expressing either WT, single mutants (S345A, S347A and T349A) or the triple mutant MLKL (N-Term) were stimulated with TNF plus zVAD and samples were probed via western blot (Figure 2c). Although lysates from cells expressing WT MLKL were positive for pMLKL, lysates from cells expressing MLKL mutated at Ser345 were negative. Unexpectedly, lysates from S347A were also negative. This is explained by the inability of the antibody to bind to pSer345, S347A peptide (Supplementary Figure 2d).

Endogenous levels of pMLKL were then examined. Upon stimulation with TNF plus zVAD, WT MEF accumulated pMLKL over time (Figure 2d). Similarly, NIH-3T3 cells expressing exogenous dimerizable RIPK3-2xFV[24,25] displayed increased positivity for pMLKL when treated either with TNF plus zVAD (Figure 2e) or dimerizer (Figure 2f).

Primary MEF are relatively insensitive to the induction of necroptosis by TNF plus zVAD and are often sensitized to death by pretreatment with Interferon β (IFNβ), possibly due to IFNβ-induced upregulation of MLKL.[11,26] Indeed, when primary WT MEF were treated with IFNβ, endogenous MLKL levels were increased (Figure 2g). Stimulation with TNF plus zVAD induced pMLKL, which was much more evident in cells primed with IFNβ (Figure 2g). Variations in the intensity and kinetics of pMLKL staining may be related to the basal levels of MLKL expression as well as other differences in the cell types used (Figure 2h). Therefore, pS345-7C6.1 antibody specifically recognizes the phosphorylation of Ser345, a critical event in RIPK3-driven MLKL activation.

GW'39B is a novel RIPK3 inhibitor. Few inhibitors for murine RIPK3 have been described: Dabrafenib, GSK'843 and GSK'872.[27,28] In order to identify a novel inhibitor of RIPK3, 8904 bioactive compounds were screened for their ability to suppress necroptosis driven by dimerizable RIPK3 (see Methods). Among 64 potential candidates, GW440139B (hereafter referred to as GW'39B) was identified as a promising inhibitor with an EC_{50} of 0.0736 μM (Supplementary Figures 3a and b).

The effects of GW'39B were tested in different cell lines. GW'39B protected SVEC (Supplementary Figure 3c) and WT MEF (Supplementary Figure 3d) from TNF plus zVAD-induced necroptosis as well as L929 cells treated with zVAD (Supplementary Figures 3e and f). NIH-3T3 cells expressing dimerizable full-length RIPK3 (RIPK3-2xFV), but not NIH-3T3 expressing RIPK3 lacking the RHIM domain (RIPK3$^{\Delta RHIM}$-2xFV), died in response to TNF plus zVAD (Supplementary Figures 3g and j), as previously reported.[24] GW'39B fully blocked necroptosis in these cells (Supplementary Figures 3g and h). Moreover, GW'39B disrupted RIPK3-MLKL complexes induced by TNF plus zVAD (Supplementary Figure 3k). GW'39B also protected human HT-29 (Supplementary Figure 3l) and RIPK3-expressing HeLa cells (Supplementary Figure 3m) from TNF plus zVAD and SMAC mimetic (LCL--161)-induced necroptosis.

Next, GW'39B was tested against TRIF-mediated necroptosis. Poly I:C plus zVAD induced necroptosis in immortalized WT MEF that was strongly reduced in the presence of GW'39B (Supplementary Figure 3n). Likewise, GW'39B significantly reduced necroptosis levels of bone marrow-derived macrophages stimulated with lipopolysaccharide (LPS) and zVAD

Figure 2 Western blot detection of RIPK3-mediated phosphorylation of MLKL at Ser345. (**a**) The reactivity of the purified antibody from the hybridoma clone pS345-7C6.1 against specific phosphorylated residues was assessed by ELISA, using different peptides (nonphosphorylated peptide (CTRL), pS345, pS347 or pT349 – see Materials and Methods for details). Data are expressed as absorbance at 640 nm (A_{640}). (**b**–**h**) Total cell lysates were tested for total MLKL and pSer345-MLKL (pMLKL) by western blot using anti-MLKL (AP14272b, Abgent) and anti-pMLKL (clone pS345-7C6.1), respectively. Actin was used as a loading control. (**b**) *Mlkl*$^{-/-}$ MEF expressing WT MLKL-FLAG (C-Term) were incubated 16 h with 1 μg/ml DOX followed by a time course (0, 60, 120 and 240 min) of 10 ng/ml TNF plus 25 μM zVAD stimulation. (**c**) *Mlkl*$^{-/-}$ MEF expressing WT, S345A, S347A, T349A or S345A/S347A/T349A (Triple) FLAG-MLKL (N-Term) were incubated 16 h in presence or absence of 1 μg/ml DOX and treated or not with 10 ng/ml TNF plus 25 μM zVAD. (**d**) Immortalized WT MEF were stimulated for the specified periods with 10 ng/ml TNF plus 25 μM zVAD. (**e** and **f**) NIH-3T3+RIPK3-2xFV cells were stimulated for the specified periods with (**e**) 10 ng/ml TNF plus 25 μM zVAD or (**f**) 10 nM Dimerizer (AP 20187). (**g**) Primary WT MEF were preincubated for 16 h in the presence or absence of 25 U/ml IFNβ and then stimulated with 10 ng/ml TNF plus 25 μM zVAD for the specified time points. (**h**) Comparison of pMLKL staining kinetics among three independently generated lines of immortalized WT MEF (A, B and C) as well as NIH-3T3+RIPK3-2xFV stimulated with 10 ng/ml TNF plus 25 μM zVAD. The asterisk (*) indicates nonspecific bands, whereas the arrowhead indicates the specific band for pMLKL

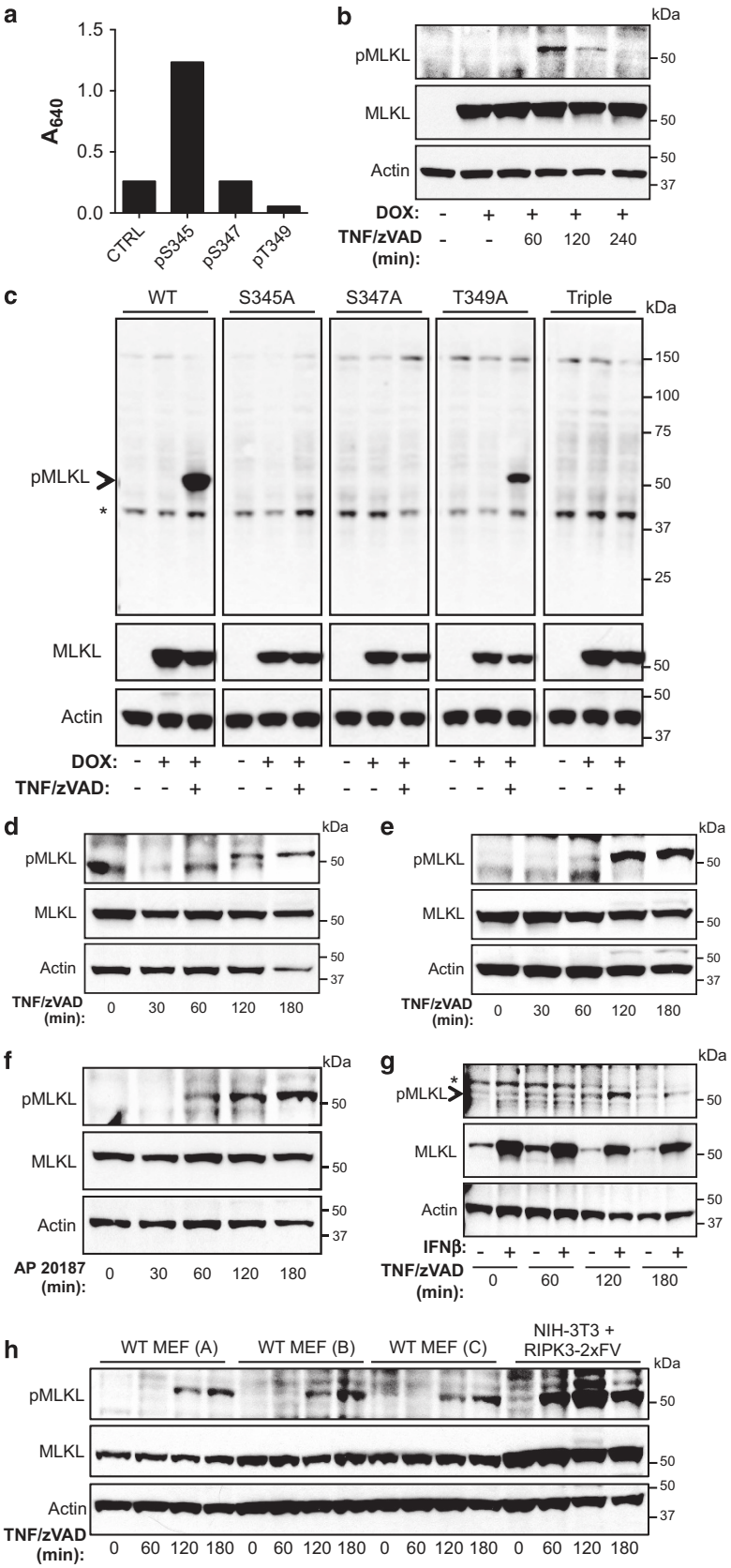
a
1.5
1.0
0.5
0.0
A640
CTRL
pS345
pS347
pT349
b
kDa
pMLKL
MLKL
Actin
50
50
50
37
DOX: - + + + +
TNF/zVAD (min): - - 60 120 240
c
WT
S345A
S347A
T349A
Triple
kDa
150
100
75
50
37
25
pMLKL
*
MLKL
Actin
50
50
37
DOX: - + + - + + - + + - + + - + +
TNF/zVAD: - - + - - + - - + - - + - - +
d
kDa
pMLKL
MLKL
Actin
50
50
50
37
TNF/zVAD (min): 0 30 60 120 180
e
kDa
pMLKL
MLKL
Actin
50
50
50
37
TNF/zVAD (min): 0 30 60 120 180
f
kDa
pMLKL
MLKL
Actin
50
50
50
37
AP 20187 (min): 0 30 60 120 180
g
kDa
pMLKL
*
MLKL
Actin
50
50
50
37
IFNβ: - + - + - + - +
TNF/zVAD (min): 0 60 120 180
h
WT MEF (A)
WT MEF (B)
WT MEF (C)
NIH-3T3 + RIPK3-2xFV
kDa
pMLKL
MLKL
Actin
50
50
50
37
TNF/zVAD (min): 0 60 120 180 0 60 120 180 0 60 120 180 0 60 120 180

(Supplementary Figure 3o) as well as RIPK3-expressing HeLa cells stimulated with poly I:C plus zVAD and SMAC mimetic (Supplementary Figure 3p).

In order to assess whether the suppressive effect of GW'39B was independent of the RIPK1–RIPK3 interactions, NIH-3T3 cells expressing RIPK3$^{\Delta RHIM}$-2xFV were stimulated with dimerizer in the presence or absence of GW'39B (Supplementary Figure 3q). Enforced RIPK3 $^{\Delta RHIM}$ oligomerization, which does not recruit RIPK1,[24,29] induced necroptosis, which was completely blocked by GW'39B (Supplementary Figure 3q).

Finally, we asked if GW'39B specifically suppresses necroptosis or can also block TNF-mediated apoptosis. GW'39B did not protect L929 cells against TNF plus cycloheximide (CHX)-induced apoptosis (Supplementary Figure 4a), but protected from necroptosis induced by zVAD (Supplementary Figures 3e and f). *Mlkl*$^{-/-}$ or *ripk1*$^{-/-}$*mlkl*$^{-/-}$ MEF, which cannot undergo necroptosis, died by apoptosis when treated with TNF plus CHX, as demonstrated by the ability of qVD ability to protect (Supplementary Figures 4b and c). GW'39B, however, did not alter the levels of cell death (Supplementary Figures 4b and c).

TNF plus CHX treatment induced a mixed cell death phenotype in NIH-3T3 expressing RIPK3-2xFV (Supplementary Figures 4d and f). Addition of qVD shifted the mode of cell death to necroptosis, which was blocked by the addition of Nec-1s (Supplementary Figures 4d and f). GW'39B, in turn, protected cells from necroptosis but shifted the cell death mode to apoptosis (Supplementary Figures 4d and f), as evidenced by the apoptotic morphology of the cells under these conditions (Supplementary Figure 4f). NIH-3T3 cells expressing RIPK3$^{\Delta RHIM}$-2xFV, which cannot undergo necroptosis, died by apoptosis induced by TNF plus CHX even in the presence of GW'39B (Supplementary Figures 4e and f).

Inhibition of RIPK3 prevents the phosphorylation of MLKL at Ser345. As MLKL phosphorylation at Ser345 is critical for the induction of RIPK3-mediated necroptosis, we examined the effects of inhibitors on this event. Treatment of *mlkl*$^{-/-}$ MEF expressing FLAG-MLKL (N-Term) with TNF plus zVAD induced the phosphorylation of MLKL at Ser345 (Figure 3a, Supplementary Figure 2b) and the inhibition of either RIPK1 by Nec-1s or RIPK3 by GSK'872 blocked it. Increasing concentrations of GW'39B similarly prevented MLKL phosphorylation in a dose-dependent manner (Figure 3a).

Similar results were observed in NIH-3T3 expressing full-length RIPK3 (Figure 3b) and immortalized WT MEF (Figure 3c). In both cases, GW'39B, as well as Nec-1s and GSK'872, prevented TNF plus zVAD-induced pMLKL (Figures 3b and c), which correlated with the ability of GW'39B to suppress necroptosis in these cells (Supplementary Figures 3d, g and h). GW'39B also prevented zVAD-induced pMLKL in L929 (Figure 3d), which again correlated with protection from necroptosis (Supplementary Figures 3e and f). GW'39B similarly ablated the phosphorylation of MLKL when cells were primed with IFNβ (Figure 3e). The effect of GW'39B on suppressing RIPK3-induced MLKL phosphorylation was also observed in the human HT-29 and RIPK3-expressing HeLa cells (Figures 3f and g) and, again, it correlated with inhibition of necroptosis (Supplementary Figures 3l and m).

Inhibition by GW'39B of Ser345 phosphorylation was also observed with TRIF-dependent stimuli. Poly I:C and zVAD treatment induced pMLKL in *mlkl*$^{-/-}$ MEF expressing FLAG-MLKL (N-Term) as well as in immortalized WT MEF (Figures 3h and i). Likewise, macrophages incubated with LPS and zVAD also displayed increased pMLKL (Figure 3j). In each case, phosphorylation of MLKL at Ser345 was blocked by GW'39B (Figures 3h and j).

To investigate whether phosphorylation of MLKL at Ser345 happens exclusively during necroptosis, WT *versus ripk1*$^{-/-}$ MEF were stimulated either under necroptotic (TNF plus zVAD) or apoptotic (TNF plus CHX) conditions and lysates were probed for pMLKL. Phosphorylation of MLKL was observed in WT MEF stimulated with TNF plus zVAD but not in *ripk1*$^{-/-}$ MEF, in agreement with the role of RIPK1 in this pathway (Figure 3k). Apoptotic signaling (TNF plus CHX) did not induce phosphorylation of MLKL in any of the cell lines (Figure 3k), rather it induced the cleavage of caspase-3, which was not affected by GW'39B (Figure 3k). Apoptosis induced by TNF plus CHX, evidenced by caspase-3 cleavage, also did not induce pMLKL in NIH-3T3 cells expressing exogenous full-length RIPK3 (Figure 3l). In contrast, TNF plus zVAD induced pMLKL without activating caspase-3 (Figure 3l). GW'39B was innocuous to apoptotic treatment but prevented necroptotic-induced MLKL phosphorylation.

Phosphorylated MLKL at serine 345 is part of the necrosome complex during necroptosis. We then characterized pMLKL in the necrosome. Addition of the cross-linking agent BMH to cell lysates revealed that, under necroptotic conditions, WT FLAG-MLKL (N-Term) formed

Figure 3 The novel RIPK3 inhibitor GW440139B (GW'39B) blocks the phosphorylation of MLKL at Ser345. (**a–l**) Total cell lysates were tested for total MLKL and pSer345-MLKL (pMLKL) by western blot using anti-murine MLKL (AP14272b, Abgent) or anti-human MLKL (M6697, Sigma) and anti-pS345-MLKL (clone pS345-7C6.1) or anti-human pS358-MLKL (Ab187091, Abcam), respectively. Actin was used as a loading control. (**a**) *Mlkl*$^{-/-}$ MEF expressing WT FLAG-MLKL (N-Term) was stimulated for 16 h with different combinations of 1 μg/ml DOX, 10 ng/ml TNF, 25 μM zVAD, 30 μM Nec-1s, 0.5 μM GSK'872 or increasing concentrations of GW'39B, as indicated. (**b**) NIH-3T3+RIPK3-2xFV or (**c**) immortalized WT MEF were incubated for 2 h with different combinations of 10 ng/ml TNF, 25 μM zVAD, 30 μM Nec-1s, 0.5 μM GW'39B or 0.5 μM GSK'872, as indicated. (**d**) Mouse L929 cells were stimulated for 4 h with 50 μM zVAD in the absence or presence of 0.5 μM GW'39B or 30 μM Nec-1s. (**e**) Primary WT MEF were primed 16 h with 25 U/ml IFNβ and incubated 2 h with or without 10 ng/ml TNF and 25 μM zVAD in the presence or absence of 0.5 μM GW'39B. (**f**) HT-29 or (**g**) RIPK3-expressing HeLa cells were incubated for 2 h with different combinations of 5 ng/ml hTNF-α, 25 μM zVAD, 5 μM LCL-161, 30 μM Nec-1s, 1.0 μM GW'39B or 1.0 μM GSK'840, as indicated. (**h**) *Mlkl*$^{-/-}$ MEF expressing FLAG-MLKL (N-Term) pretreated for 16 h with 1 μg/ml DOX or (**i**) immortalized WT MEF were incubated for 2 h in the presence of 100 μg/ml poly I:C and/or 25 μM zVAD and/or 0.5 μM GW'39B or 30 μM Nec-1s. (**j**) Immortalized macrophages (iMACs) were cultured for 2 h with 50 ng/ml LPS in the absence or presence 25 μM zVAD and/or 0.5 μM GW'44B. (**k**) WT or *ripk1*$^{-/-}$ MEF or (**l**) NIH-3T3s (RIPK3-2xFV) were incubated for 2 h in the presence of 10 ng/ml TNF plus 25 μM zVAD or alternatively, 10 ng/ml TNF plus 0.5 μg/ml CHX. 0.5 μM GW'39B was added to some samples. After the treatments, cell lysates were analyzed by western blot. Cleaved Caspase 3 (cCasp 3) was assessed as an indicator of apoptosis. Where indicated, the asterisk (*) indicates nonspecific bands, whereas the arrowhead indicates the specific band for pMLKL

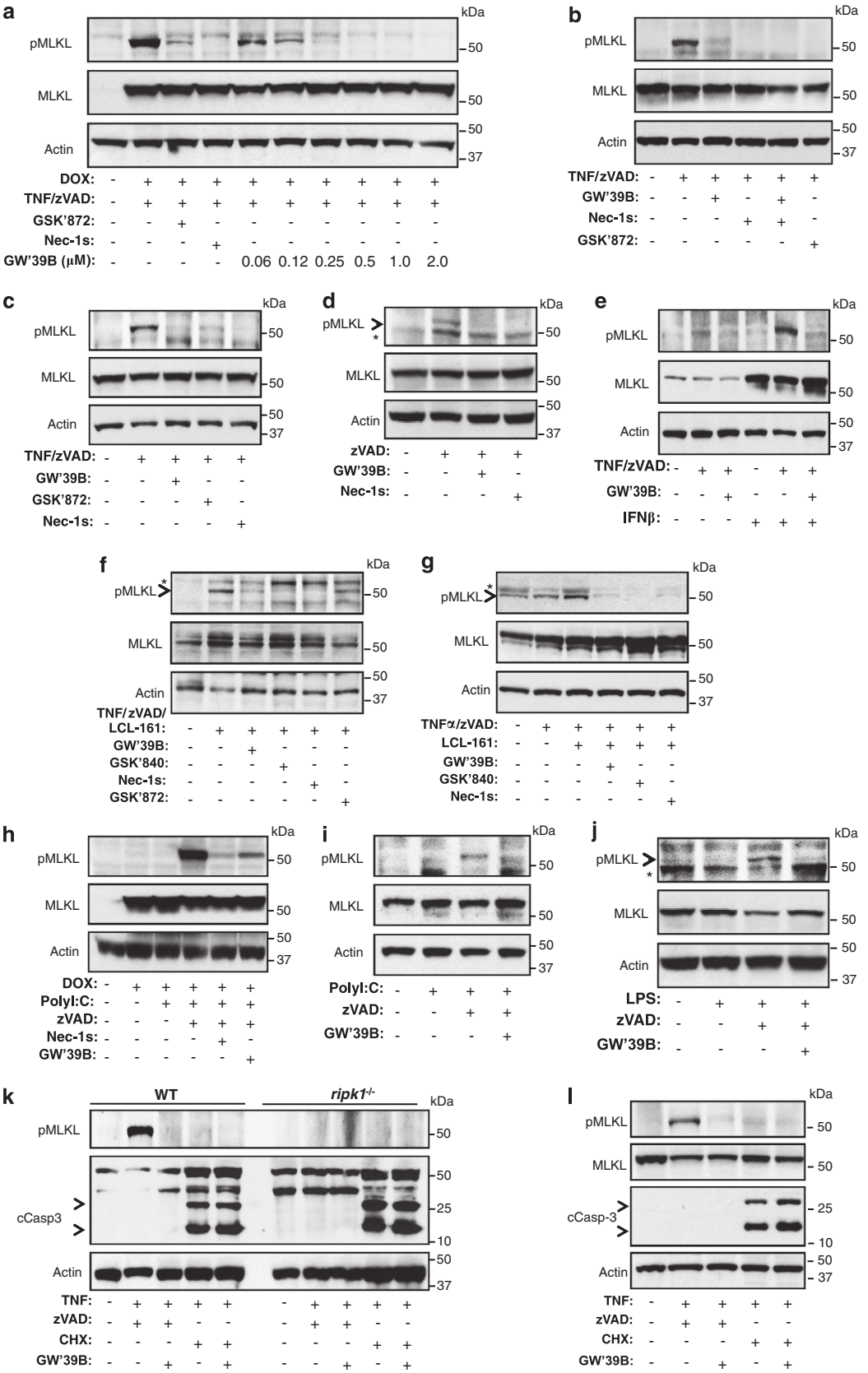
a
pMLKL
MLKL
Actin
kDa
50
50
50
37
DOX: - + + + + + + + + +
TNF/zVAD: - + + + + + + + + +
GSK'872: - - + - - - - - - -
Nec-1s: - - - + - - - - - -
GW'39B (μM): - - - - 0.06 0.12 0.25 0.5 1.0 2.0
b
pMLKL
MLKL
Actin
kDa
50
50
50
37
TNF/zVAD: - + + + + +
GW'39B: - - + - + -
Nec-1s: - - - + + -
GSK'872: - - - - - +
c
pMLKL
MLKL
Actin
kDa
50
50
50
37
TNF/zVAD: - + + + +
GW'39B: - - + - -
GSK'872: - - - + -
Nec-1s: - - - - +
d
pMLKL
*
MLKL
Actin
kDa
50
50
50
37
zVAD: - + + +
GW'39B: - - + -
Nec-1s: - - - +
e
pMLKL
MLKL
Actin
kDa
50
50
50
37
TNF/zVAD: - + + - + +
GW'39B: - - + - - +
IFNβ: - - - + + +
f
pMLKL
*
MLKL
Actin
kDa
50
50
50
37
TNF/zVAD/
LCL-161: - + + + + +
GW'39B: - - + - - -
GSK'840: - - - + - -
Nec-1s: - - - - + -
GSK'872: - - - - - +
g
pMLKL
*
MLKL
Actin
kDa
50
50
50
37
TNFα/zVAD: - + + + + +
LCL-161: - - + + + +
GW'39B: - - - + - -
GSK'840: - - - - + -
Nec-1s: - - - - - +
h
pMLKL
MLKL
Actin
kDa
50
50
50
37
DOX: - + + + + +
PolyI:C: - - + + + +
zVAD: - - - + + +
Nec-1s: - - - - + -
GW'39B: - - - - - +
i
pMLKL
MLKL
Actin
kDa
50
50
50
37
PolyI:C: - + + +
zVAD: - - + +
GW'39B: - - - +
j
pMLKL
*
MLKL
Actin
kDa
50
50
50
37
LPS: - + + +
zVAD: - - + +
GW'39B: - - - +
k
WT
ripk1-/-
pMLKL
cCasp3
Actin
kDa
50
50
25
10
50
37
TNF: - + + + + - + + + +
zVAD: - + + - - - + + - -
CHX: - - - + + - - - + +
GW'39B: - - + - + - - + - +
l
pMLKL
MLKL
cCasp-3
Actin
kDa
50
50
25
10
50
37
TNF: - + + + +
zVAD: - + + - -
CHX: - - - + +
GW'39B: - - + - +

oligomers, which were prevented by co-treatment with GW'39B or Nec-1s (Figure 4a, upper and middle panels). Interestingly, pMLKL was highly enriched in the oligomer fractions when compared with the monomers (Figure 4a, bottom panel).

Next, pMLKL was immunoprecipitated using the anti-pS345-MLKL monoclonal antibody after TNF plus zVAD stimulation in the presence or absence of GSK'872. Total MLKL was detected only in cells treated with DOX and TNF plus zVAD but not in cells treated only with DOX (Figure 4b, middle panel). Inhibition of RIPK3 kinase activity by GSK'872 attenuated the detection of MLKL (Figure 4b, middle panel), likely due to decreased pMLKL levels in the input fraction (Figure 4b, lower panel). In parallel, immunoprecipitation of total FLAG-MLKL followed by detection of pMLKL confirmed that pMLKL is only present upon TNF plus zVAD treatment. RIPK3 inhibition by GSK'872 reduced the amount of immunoprecipitated pMLKL (Figure 4b, upper panel).

Immunoprecipitation of pMLKL in cells treated with DOX and TNF plus zVAD co-precipitated RIPK3 and RIPK1, indicating that pMLKL is part of the active RIPK1–RIPK3–MLKL necrosome complex (Figure 4c, middle panel). Addition of GW'39B strongly blocked the phosphorylation of MLKL (Figure 4c, input fraction), which in turn resulted in decreased co-precipitation of pMLKL with RIPK1 and RIPK3 (Figure 4c, middle panel). Total FLAG-MLKL immunoprecipitation in cells treated under the same conditions showed that GW'39B partially disrupted the formation of the necrosome complex containing RIPK1, RIPK3 and MLKL (Figure 4c, upper panel), suggesting that GW'39B decreased the interaction between RIPK3 and MLKL (see Discussion).

As active RIPK3 can directly interact with MLKL,[2,20,30] and this interaction can be partially suppressed when the RIPK3 kinase activity is inhibited (Figure 4b), we asked whether the triple (S345A, S347A and T349A) MLKL mutant interacts with RIPK3 during necroptosis. As expected, upon TNF plus zVAD stimulation, pMLKL was only detected in WT MLKL-expressing cells treated (Figure 4d, input fraction). As a consequence, immunoprecipitation of pMLKL resulted in co-precipitation of RIPK3 only in WT MLKL-expressing cells treated with TNF plus zVAD, but not in the triple mutant-expressing cells (Figure 4d, middle panel). Importantly, immunoprecipitation of total MLKL revealed that both the WT and the triple-mutant MLKL interact at similar levels with RIPK3 (Figure 4d, upper panel), suggesting that the MLKL residues Ser345, Ser347 and Thr349 are dispensable for the RIPK3 and MLKL interaction. Interestingly, the inhibition of RIPK3 kinase activity (GW'39B) disrupted the interaction between MLKL and RIPK3 to the same extent in both cell lines (Figure 4d, upper panel). It is likely that GW'39B inhibition of autophosphorylation of RIPK3 results in decreased interaction with MLKL, as previously studies have demonstrated that MLKL binding to RIPK3 depends on the RIPK3 kinase activity.[2]

Therefore, during necroptosis, pMLKL is found in the oligomeric necrosome complex and the inhibition of RIPK3 kinase activity attenuates the interaction between RIPK3 and MLKL. However, the phosphorylation state of MLKL at the activation loop does not impact its binding to RIPK3.

Phosphorylation of Ser345 licenses MLKL to plasma membrane translocation. To directly address whether RIPK3-mediated phosphorylation of MLKL at Ser345 affects the cellular localization of pMLKL, we performed confocal microcopy analysis of *mlkl*$^{-/-}$ MEF expressing WT FLAG-MLKL (N-Term). Upon expression, MLKL was mainly localized in the cytoplasm and cells did not stain for pMLKL (Figure 5a). Upon TNF plus zVAD treatment, pMLKL staining was evident and predominantly localized at the plasma membrane (Figure 5a, Supplementary Figure 5c). Addition of GW'39B dramatically decreased pMLKL staining and blocked MLKL translocation to the plasma membrane (Figure 5a, Supplementary Figure 5c). Image analysis for the intensity of each channel through a line encompassing cytoplasm bounded by plasma membrane, 3D reconstruction and Pearson's analysis of pMLKL distribution between cytosol and plasma membrane were performed (Figures 5b and c, Supplementary Figures 5a and b).

These findings suggest that the interaction with RIPK3 is not sufficient for MLKL to translocate to the plasma membrane; instead MLKL must be phosphorylated at Ser345 by RIPK3 to relocate and execute necroptosis. We therefore addressed the localization of the MLKL mutants that are unable to engage necroptosis (Figure 1) under the same conditions described above. As expected, after TNF plus zVAD stimulation, pMLKL was only detected in WT MLKL, but not the double or the triple mutants (Figure 5d). Under these conditions, the mutants did not translocate to the plasma membrane (Figure 5e, Supplementary Figure 5c). Substitution of Thr349 with alanine, which did not affect the ability of MLKL to induce necroptosis (Figure 1b), also did not impact on its localization after RIPK3-mediated activation (Figure 5f).

Altogether, we provide a mechanism in which RIPK3-mediated phosphorylation of MLKL in the activation loop at Ser345 is required to activate MLKL in a process that involves the plasma translocation of MLKL to execute necroptosis. The addition of an N-terminal FLAG disrupts the ability of MLKL to permeabilize and execute necroptosis[11] without affecting its translocation to the plasma membrane upon phosphorylation.

Figure 4 RIPK1/RIPK3/MLKL complex formation does not depend on the phosphorylation of MLKL at Ser345. (**a**) *Mlkl*$^{-/-}$ MEF expressing FLAG-MLKL (N-Term) were cultured 16 h with 1 μg/ml DOX followed by 4 h treatment with 10 ng/ml TNF plus 25 μM zVAD in the absence or presence of 0.5 μM GW'39B or 30 μM Nec-1s. Cell lysates were incubated in the absence or presence of 125 μM BMH cross-linker and the formation of higher molecular complexes was analyzed by western blot. (**b** and **c**) *Mlkl*$^{-/-}$ MEF expressing FLAG-MLKL (N-Term) were cultured 16 h with 1 μg/ml DOX followed by 2 h treatment with 10 ng/ml TNF plus 25 μM zVAD in the absence or presence of (**b**) 0.5 μM GSK'872 or (**c**) 0.5 μM GW'39B. Total MLKL or pMLKL was immunoprecipitated by beads coupled with anti-FLAG or anti-pS345-MLKL, respectively (see Materials and Methods). Independent blots were probed with antibodies to RIPK1, RIPK3, FLAG, MLKL, pMLKL and actin as loading control. (**d**) *Mlkl*$^{-/-}$ MEF expressing WT or the triple mutant (S345A/S347A/T349A) FLAG-MLKL (N-Term) were cultured 16 h with 1 μg/ml DOX followed by 2 h treatment with 10 ng/ml TNF plus 25 μM zVAD in the absence or presence of 0.5 μM GW'39B. After treatment, the cell lysates were analyzed by western blot

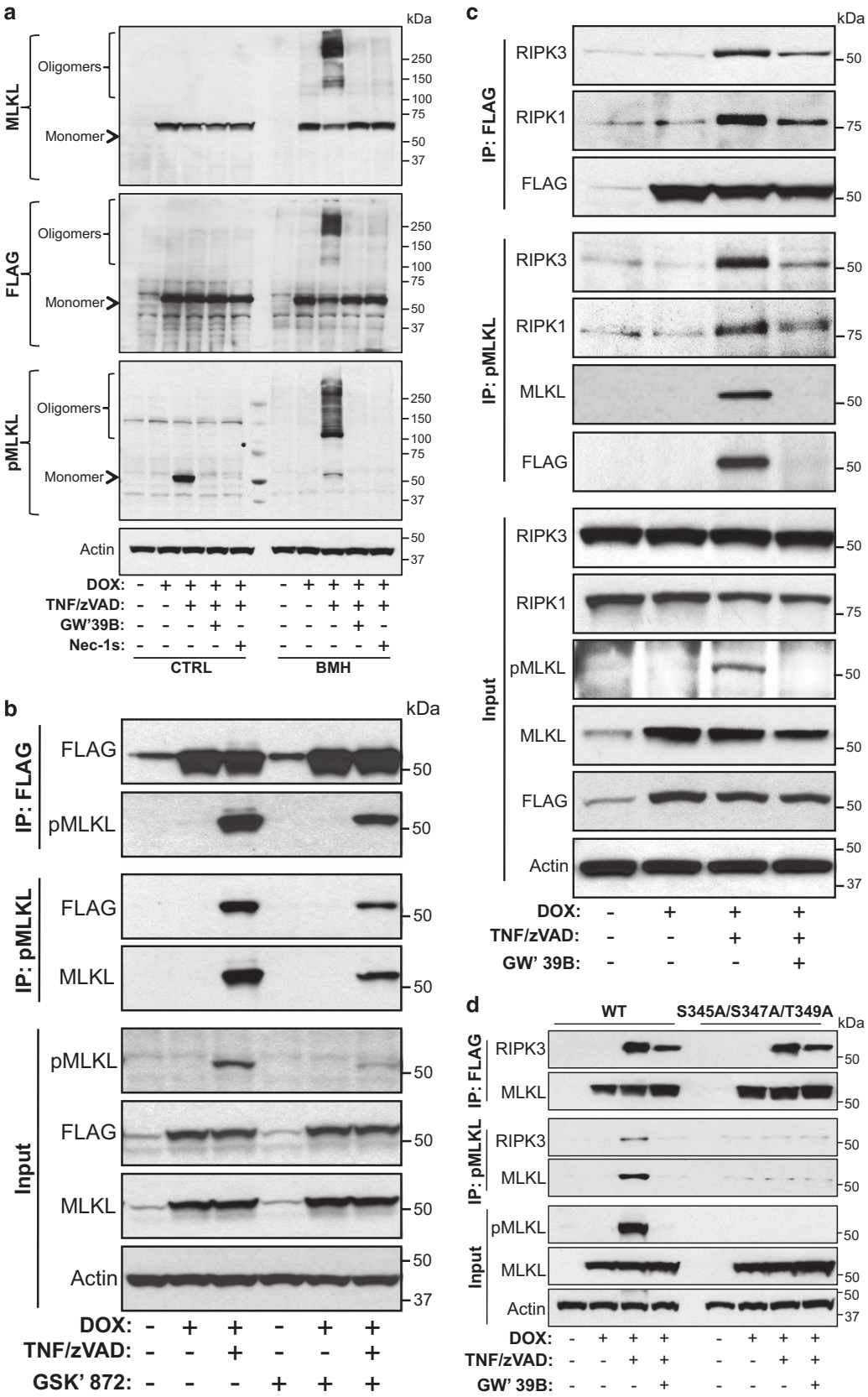
a
kDa
MLKL
Oligomers
Monomer
FLAG
Oligomers
Monomer
pMLKL
Oligomers
Monomer
250
150
100
75
50
37
Actin
50
37
DOX: - + + + + - + + + +
TNF/zVAD: - - + + + - - + + +
GW'39B: - - - + - - - - + -
Nec-1s: - - - - + - - - - +
CTRL
BMH
b
kDa
IP: FLAG
FLAG
pMLKL
IP: pMLKL
FLAG
MLKL
Input
pMLKL
FLAG
MLKL
Actin
50
37
DOX: - + + - + +
TNF/zVAD: - - + - - +
GSK' 872: - - - + + +
c
kDa
IP: FLAG
RIPK3
RIPK1
FLAG
IP: pMLKL
RIPK3
RIPK1
MLKL
FLAG
Input
RIPK3
RIPK1
pMLKL
MLKL
FLAG
Actin
50
75
37
DOX: - + + +
TNF/zVAD: - - + +
GW' 39B: - - - +
d
WT
S345A/S347A/T349A
kDa
IP: FLAG
RIPK3
MLKL
IP: pMLKL
RIPK3
MLKL
Input
pMLKL
MLKL
Actin
50
37
DOX: - + + + - + + +
TNF/zVAD: - - + + - - + +
GW' 39B: - - - + - - - +

Discussion

RIPK3 can phosphorylate several residues in the activation loop of MLKL, including Ser345, Ser347 and Thr349.[3] In this study, we found that mutation of Ser345 to alanine reduced the ability of MLKL to induce necroptosis. Ser347 has an accessory role to that of Ser345, as the additional mutation of this residue rendered MLKL completely ineffective for necroptosis. These residues correspond to the Ser357 and Ser358 of the human MLKL, whose phosphorylation was previously shown to be essential for human MLKL oligomerization and engagement of necroptosis.[16]

The phospho-mimic S345D, S347D resulted in a constitutively active MLKL. Consistently, overexpression of the single mutant S345D, as well as mutants in which the hydrogen bond between the residues K219 and Q343 in the activation loop was disrupted, also resulted in aberrant MLKL activation and cell death.[3] Here we further found that S345D, S347D MLKL does not require the presence of endogenous RIPK3 or MLKL. This is in agreement with studies showing that the S345D mutant induces liposome permeabilization.[16] These data support the idea that phosphorylation at Ser345 by RIPK3 induces conformational changes in the activation loop (likely by disrupting the hydrogen bond between Glu343 and Lys219) to activate MLKL.[3,21] Our findings further demonstrate that this event is sufficient for MLKL activation and function, suggesting that additional posttranslational modifications of MLKL are not essential for its activation.

Using an antibody that recognizes pS345-MLKL and the MLKL mutants at Ser345, Ser347 and/or Thr349, we found that the lack of phosphorylation at these residues did not impact the interaction between MLKL and RIPK3 in the necrosome. This is consistent with a previous observation that the kinase domain of RIPK3 retains the ability to bind to the triple mutant (S345A, S347A and T349A) MLKL kinase-like domain.[20] However, RIPK3 activity, likely RIPK3 autophosphorylation, is required for the binding of MLKL.[20,30]

Using the same approach, we found that mutations at Ser345 and Ser347, but not at Thr349, to alanines completely abrogated the translocation of MLKL from the cytoplasm to the plasma membrane, indicating that the phosphorylation of MLKL at these residues precedes and is necessary for its relocation. Similar results were found for human MLKL; T357A, S358A mutations prevented the oligomerization and translocation of hMLKL.[16]

It was previously reported that MLKL is acetylated at Lys77[22] and that the double mutation, E76A, K77A, strongly attenuated the ability of the truncated MLKL (1–180) to induce necroptosis.[18] However, the substitution of Lys77 for an arginine (K77R) or an alanine (K77A) did not alter the activity of MLKL upon TNF plus zVAD treatment, suggesting that the lack of acetylation of MLKL at this residue does not affect its necroptotic function. As the instances in which MLKL is acetylated are still unknown, it is yet to be tested whether this posttranslational modification has any role in the physiology of MLKL.

As the kinase activity of RIPK1 not only promotes necroptosis but, in some cases, can induce apoptosis,[31–33] targeting downstream of RIPK1 by suppressing RIPK3 function might be an attractive alternative for a more specific suppression of the necroptotic pathway. Curiously, elevated doses of two newly described RIPK3 inhibitors (GSK'843 and GSK'872) were able to fully block necroptosis but, at the same time, both induced apoptosis.[27,34] Similar results were seen in cells that expressed a kinase-dead RIPK3 (D161N),[34] or under conditions in which MLKL was silenced;[35] in all of these cases, kinase-inhibited RIPK3 mediates the recruitment of a complex comprised of RIPK1–FADD–FLIP, which recruits and activates caspase-8. In this study, we described a new molecule, GW'39B, which blocks RIPK3-mediated MLKL phosphorylation both in murine and human cells, thus inhibiting MLKL oligomerization. Although the structural core of this compound is very similar to the GSK'872, it is yet to be determined whether high concentrations of GW'39B also induce apoptosis.

Strong upregulation of RIPK3 has been shown in inflammatory diseases,[36] opening the possibilities for therapeutic interventions. Supporting this idea, biopsies of liver from patients suffering drug-induced liver injury have higher levels of phosphorylated MLKL at the Ser358[28] and patients affected by toxic epidermal necrolysis, which present extensive keratinocyte death in the epidermis,[37] have increased levels of RIPK3 and phosphorylated MLKL.[38] Altogether, these findings suggest opportunities for RIPK3 inhibitors in the treatment of diseases where high RIPK3 kinase activity promotes human pathologies, also including steatohepatitis[36] and Gaucher's disease.[39]

Materials and Methods

Cell lines. Primary MEFs were generated by mating animals of the required genotypes and harvesting embryos at E12–E14 based on palpation. Following removal of the head and fetal liver, a single-cell suspension was generated from the remaining parts of the embryo and plated in DMEM supplemented with 10% FBS, L-glutamine, pen/strep, 55 μM β-mercaptoethanol, 1 mM sodium pyruvate and nonessential amino acids (GIBCO). All experiments on primary MEF were performed on cells no older than passage 3, and data shown represent experiments using independently derived MEF. *Mlkl*$^{-/-}$, *ripk1*$^{-/-}$, *ripk1*$^{-/-}$*mlkl*$^{-/-}$

Figure 5 Phosphorylated MLKL at Ser345 is localized at the plasma membrane. (**a**) *Mlkl*$^{-/-}$ MEF expressing WT FLAG-MLKL (N-Term) were cultured 16 h with 1 μg/ml DOX followed by 4 h treatment with 10 ng/ml TNF plus 25 μM zVAD in the absence or presence of 0.5 μM GW'39B. Cells were washed, fixed, permeabilized and stained using anti-FLAG (green) or anti-pS345-MLKL (red). F-actin (white) and nuclei (DAPI) were stained with 0.1 μM phalloidin and 1 μg/ml Hoechst, respectively. Images were acquired by confocal microscopy (see Material and Methods). Merged images illustrate DAPI/pMLKL/FLAG fluorescence. (**b**) Representative histogram for the pMLKL (red line) and FLAG (green line) intensities along a line drawn across an area encompassing cytoplasm bounded by plasma membrane. (**c**) Pearson's correlation for pMLKL and FLAG between cytosol and membrane. (**d**) Western blot analysis of *mlkl*$^{-/-}$ MEF expressing WT, double (S345A/S347A) or triple mutant (S345A/S347A/T349A) FLAG-MLKL (N-Term). Cells were treated 16 h with 1 μg/ml DOX followed treatment of 4 h with 10 ng/ml TNF and 25 μM zVAD in the absence or presence of 0.5 μM GW'39B. Western blots were probed with antibodies to pMLKL, total MLKL and actin as loading control. (**e** and **f**) MEF expressing different MLKL mutants were treated as in **a** and the treatment condition with DOX plus TNF and zVAD is shown (refer to Supplementary Figure 5 for additional treatment conditions). The distribution of pMLKL, MLKL and actin were quantified for individual pixels along a line drawn across an area encompassing cytoplasm bounded by plasma membrane and shown as histograms (right panel). Scale bars in **a** and **e** represent 20 μm and in **f** 10 μm

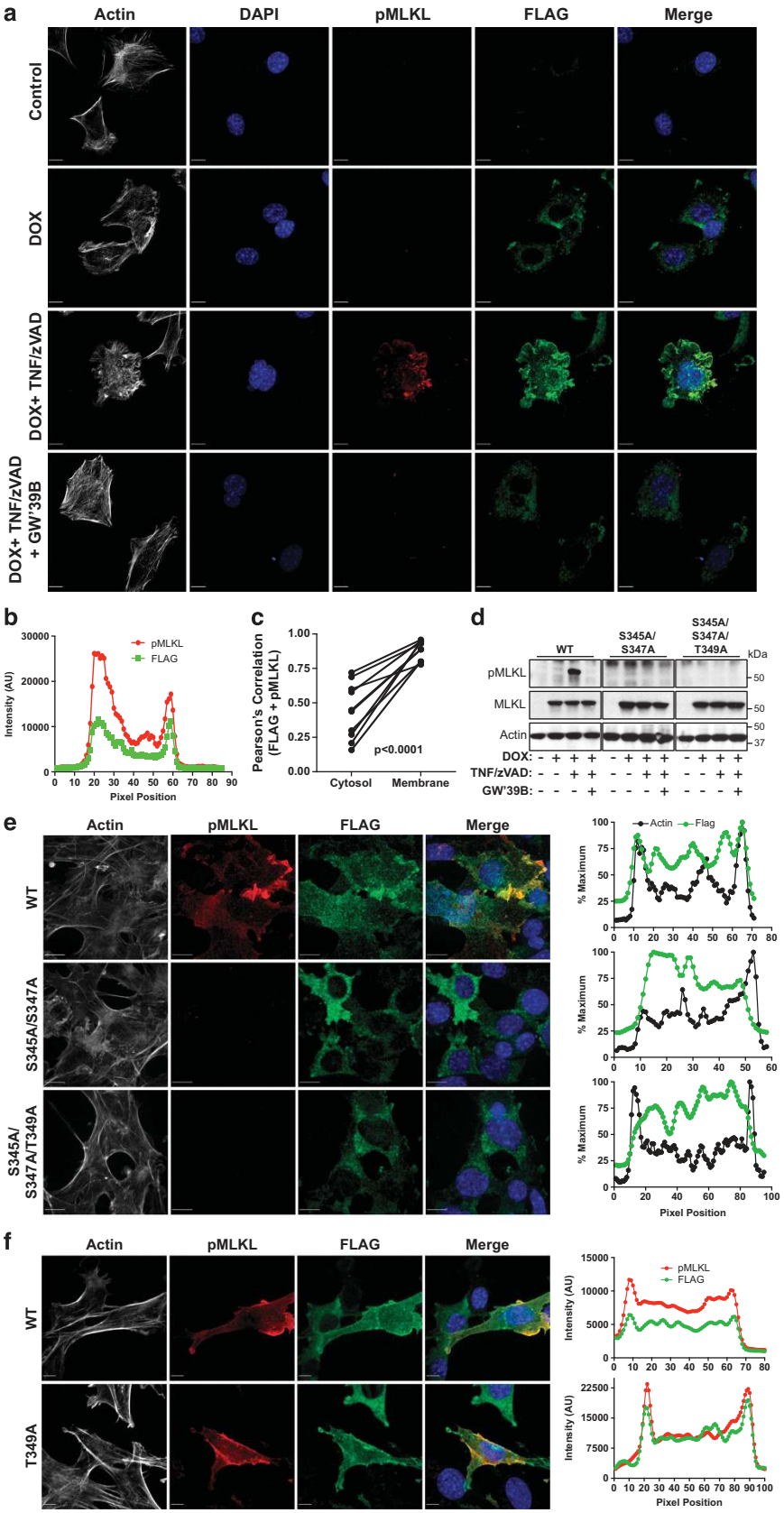
a
Actin
DAPI
pMLKL
FLAG
Merge
Control
DOX
DOX+ TNF/zVAD
DOX+ TNF/zVAD + GW'39B
b
pMLKL
FLAG
Intensity (AU)
Pixel Position
c
Pearson's Correlation (FLAG + pMLKL)
p<0.0001
Cytosol
Membrane
d
WT
S345A/ S347A
S345A/ S347A/ T349A
kDa
pMLKL
MLKL
Actin
DOX:
TNF/zVAD:
GW'39B:
e
WT
S345A/S347A
S345A/ S347A/T349A
Actin
Flag
% Maximum
Pixel Position
f
WT
T349A
Intensity (AU)
Pixel Position

or *ripk3*$^{-/-}$*mlkl*$^{-/-}$ primary MEF were immortalized with SV40 large T antigen, and maintained in DMEM as indicated above. NIH-3T3 cells expressing RIPK3-2xFV or RIPK3$^{\Delta RHIM}$-2xFV, with or without amino-terminal (N-Term) FLAG-tag were previously described.[24,25] Human adenocarcinoma HT-29 and RIPK3-expressing HeLa cells were cultured using the same conditions described above. RIPK3-expressing HeLa cells were generated by antibiotic selection of zeocin-resistant cells that stably express full-length human RIPK3 under the control of a 5'LTR promoter in a LZRS cassette. Bone marrow-derived macrophages were generated from bone marrow progenitors obtained from littermates as described.[40] In brief, cells were cultured in RPMI 1640 medium containing 10% heat-inactivated FBS, 2 mM L-glutamine, 10 mM Hepes buffer, 50 μg/ml penicillin, nonessential amino acids and GM-CSF (315-03; Peprotech, Rocky Hill, NJ, USA). Immortalized macrophages were generated by infection of fresh bone marrow cells with J2 retrovirus.

Compounds, antibodies and cytokines. Antibodies used for western blotting were: anti-RIPK1 (clone D94C12; Cell Signaling, Danvers, MA, USA), anti-RIPK3 (14401 s; Cell Signaling), anti-FLAG (F7425; Sigma, St. Louis, MO, USA), anti-actin (clone C4; Santa Cruz Biotechnologies, Dallas, TX, USA), anti-cleaved caspase-3 (9662; Cell Signaling), anti-MLKL (AP14272b; Abgent, San Diego, CA, USA), anti-human phospho-MLKL (ser358) (ab187091; Abcam, Cambridge, MA, USA), anti-human MLKL (M6697, Sigma). The murine cytokines used were: mTNF (315-01 A; Peprotech) and mIFNβ (12400-1; PBL Assay Science, Piscataway, NJ, USA). Human recombinant TNF-α (300-01 A) was acquired from Peprotech. The SMAC mimetic and inhibitor of IAP (LCL-161) came from Chemietek (Indianapolis, IN, USA). Poly I:C (NBP2-25288) was acquired from Novus Biologicals (Littleton, CO, USA). RIPK1 Inhibitor II, 7-Cl-O-Nec-1 (Nec-1s, 504297) came from Calbiochem (Billerica, MA, USA), zVAD-fmk (A1902) and Q-VD-OPh (qVD, A8165) came from Apexbio (Houston, TX, USA). DOX (631311) and Homodimerizer (AP 20187, 635060) were obtained from Clontech (Mountain View, CA, USA). CHX (C7698) came from Sigma and cross-linker bis(maleimido) hexane (BMH, 22330) from Thermoscientific (Rockford, IL, USA). The RIPK3 inhibitors GSK2399872B (GSK'872), GSK2791840B (GSK'840) and GW440139B (GW'39B) were provided by GlaxoSmithKline (Research Triangle Park, NC, USA). All other reagents used were from Sigma or of the highest grade available.

Generating a murine MLKL monoclonal antibody against phosphoserine 345 (S345-MLKL). *Mlkl*$^{-/-}$ mice were kindly provided by Warren Alexander.[3] In brief, 6–8-week-old *mlkl*$^{-/-}$ (C57BL/6) mice were immunized (200 μl/mouse i.p.) with 50 μg of KLH-conjugated peptide containing the phosphorylated Ser345 (pS345; GFELSKTQNS*ISRTAKST) dissolved (1 : 1v/v) in PBS per animal in an emulsion with complete Freund's adjuvant (F5881; Sigma) for the initial injection and with incomplete Freund's adjuvant for subsequent boosts. Mice were bled 2 weeks following each boost and sera antibody titers tested by ELISA against the unconjugated peptides, including the nonphosphorylated and phosphorylated forms pS345, pS347 (GFELSKTQNSIS*RTAKST) and pT349 (GFELSKTQNSISRT*AKST). The animal presenting highest titers for the pS345 and lowest titer against the others was selected. Four weeks following the last boost, a final boost with 50 μg/200 μl of pS345 in PBS was split between i.v. and i.p injection. Four days later, the mouse was euthanized and splenectomy was performed. Single-cell suspensions of splenocytes were mixed with an equal number of X63-Ag-8.653 mouse myeloma cells and fused using an electrofusion system (Cyto Pulse Sciences, Inc, Holliston, MA, USA). Fused cells were selected usin, USAg HAT media (StemCell Technologies, Vancouver, BC, Canada). Single-cell cloning was performed and clone pS345-7C6.1 was selected for further analysis. Also, pS345-7C6.1 was tested using a modified version of pS345 peptide, where the Ser347 was substituted by alanine (pS345/S347A; GFELSKTQNS*IARTAKST).

Detection of phosphorylated S345-MLKL by ELISA. In order to test the reactivity of pMLKL-S345 (clone 7C6.1), each peptide (indicated above) was precoated into ELISA plates. In brief, 75 μl of the respective peptide (10 μg/ml in PBS) were added to each well of a 96-well Nunc MaxiSorp flat-bottom ELISA plate and allowed to bind for 1 h at RT. The plate was washed 1 × with washing buffer (WB; 1 × PBS containing 0.05% Tween-20) and then blocked with 300 μl of 1% fraction V BSA in PBS for 1 h at RT. Then, plates were washed 1 × with WB, and 75 μl of antibody solutions (supernatants for screening the clones during hybridoma selection or 1 μg/ml purified antibody) were added to the blocked wells. ELISA plates were incubated 1 h at RT and then washed 3 × with WB. An anti-mouse IgG HRP secondary antibody (Southern Biotech, Birmingham, AL, USA) was diluted 1 : 5000 in blocking buffer, 75 μl was added to each well and allowed to incubate at RT for 30 min. ELISA plates were washed 3 × with WB, and 75 μl of a two-component TMB substrate system (KPL, Gaithersburg, MD, USA) was added to each well. After 15 min incubation at RT, absorbance was recorded at 640 nm.

Detection of phosphorylated S345-MLKL by western blot. Cell lysates were generated using RIPA buffer containing protease and phosphatase inhibitors (Roche, Indianapolis, IN, USA). Proteins (30–50 μg) were loaded and run in 4–12% SDS-PAGE precasted gels (Bio-Rad, Hercules, CA, USA) and then transferred to nitrocellulose membranes (162-0115; Bio-Rad). Membranes were blocked in 2% BSA in Tris-buffered saline containing 0.1% (v/v) Tween-20 (TBST) for at least an hour. Then, dilutions of 0.5–1 μg/ml of the monoclonal anti-pS345-MLKL (clone 7C6.1) in 2% BSA in TBST, were incubated 2 h at room temperature or 4 °C overnight. Bound antibodies were detected with HRP-conjugated secondary antibodies and an ECL system.

Drug screening for RIPK3 inhibitors. NIH-3T3 cells expressing GFP-2A-RIPK3-2xFV were grown in DMEM (11971-025; GIBCO) supplemented with 10% FBS, L-glutamine (25030-081), penicillin and streptomycin (15140-122) and sodium pyruvate (11360-070). All 37 °C incubations were carried out in Liconic STR240 incubators and all 25 °C incubations were carried out in Liconic LPR240 incubators integrated on a High Resolution Engineering screening system. Cells (2500) in 25 μl of media were plated into each well of a Costar (8804BC) 384-well tissue-culture-treated white plate with a flat bottom. The cells were then grown for 18 h overnight at 37 °C with 5% CO_2. Cells were first treated with compound using either a V&P Scientific 10H pintool for primary screening, or a V&P Scientific 100H pintool for dose–response screening. After compound addition, the cells were returned to 37 °C with 5% CO_2 for 3 h. Cells were then treated with 5 nM dimerizer (AP 20187) using a V&P Scientific 10H pintool and returned to 37 °C and 5% CO_2 for an additional 3 h. Cells were then removed from incubation and equilibrated to 25 °C for 30 min before the addition of 25 μl of Promega Cell Titer-Glo (G755B and G756B). All plates were then incubated for 15 min at 25 °C before luminescence was measured using a Perkin Elmer Envision plate reader. Screening data were analyzed using the St Jude Robust Investigation of Screening Experiments (RISE) software. The average Z' for the screen was 0.825 with a 30-fold signal window. Thirty-four plates containing bioactive compounds, including FDA-approved drugs with a total of 8904 compounds (4359 unique) were screened and 64 hits were detected with at least 20% cell death activity of cells untreated with 5 nM dimerizer, generating a hit rate of 0.7%. Of the 64 hits from the primary screen, 36 were unique, which were further analyzed in a dose–response format. All dose–response curves were generated in RISE using a standard four-parameter curve-fit formula.

Treatment of MEF and immunoprecipitation of MLKL. Full-length MLKL was expressed in *mlkl*$^{-/-}$ MEF by cloning FLAG-MLKL (N-Term) or MLKL-FLAG (C-Term)[11] into the DOX-inducible vector pRetroX-TRE3G, transfected into cells and selected with puromycin, then induced according manufacturer's instructions (Clontech). In brief, after 24 h of MLKL expression induced via 1 μg/ml DOX, MEF expressing the FLAG-MLKL construct were incubated 2 h with 10 ng/ml TNF, 25 μM zVAD in presence or absence of 0.5 μM GSK'872, 0.5 μM GW'49B or 30 μM Nec-1s. After treatment, cell lysates were generated using a lysis buffer containing: 50 mM Tris pH 7.4, 150 mM NaCl, 1 mM EDTA, 0.5% NP-40, and containing protease and phosphatase inhibitors (Roche). FLAG immunoprecipitation was performed using anti-FLAG beads according to the manufacturer's instructions (Sigma, F2426). Alternatively, anti-pS345-MLKL was conjugated with Protein A/G PLUS-Agarose (SC-2003; Santa Cruz Biotechnologies), and then immunoprecipitations were performed overnight at 4 °C by incubating the antibody-conjugated beads with cell lysates. Elution of immunoprecipitates was performed by addition of 0.2 M glycine (pH = 2.5) followed by neutralization with Tris-HCl buffer (pH = 7.4).

Analysis of MLKL oligomerization. *Mlkl*$^{-/-}$ MEF expressing FLAG-MLKL (N-Term) were cultured 16 h in presence of DOX and then incubated 4 h with 10 ng/ml TNF plus 25 μM zVAD in combination of 0.5 μM GW'39B or 30 μM Nec-1s. Cell lysates were obtained as described for immunoprecipitations. Cell lysates (50 μl) were incubated 10 min in absence or presence of 125 μM BMH and the reactions were stopped by incubation for 5 min with 50 mM DTT. Samples were analyzed by western blot as indicated above.

Site-specific mutagenesis of the activation loop of mouse MLKL. Using the Quikchange II XL mutagenesis kit (200522-5; Agilent Technologies, Santa Clara, CA, USA), site-specific mutagenesis was performed using as templates either N-Term or C-Term FLAG-MLKL constructs. In brief, the residues Ser345, Ser347 or Thr349 were substituted by alanines in every combination, including the single, double and triple mutants. Also, a double mutant replacing both residues Ser345 and Ser347 by aspartic acid (S345D, S347D) was created.

Cell death assay. Following treatment, cells were collected and resuspended in PBS containing 1 μg/ml propidium iodide (PI). Alternatively, cells were stained with AnnexinV-APC and PI and the percentage of cell death was calculated by the sum of AnnexinV$^+$PI$^+$ and AnnexinV$^+$PI$^-$. Cells were analyzed by flow cytometry using either FACSscan or FACsCalibur II and Cellquest Pro software (BD Biosciences, San Jose, CA, USA). Alternatively, cell death was monitored in real time using an Incucyte FLR or Zoom imaging systems (Essen Bioscience, Ann Arbor, MI, USA). In brief, cells were plated in medium containing 25 nM of the membrane impermeant dye Sytox Green (S7020; Invitrogen, Eugene, OR, USA). At the end point, all cells were stained with 100 nM of the membrane permeant dye Syto24 Green (S7559; Invitrogen). Cell death was quantified using the Incucyte image analysis software (Essen Bioescience). Data were expressed as percentages of the ratio between Sytox Green/Syto24 (% Sytox Green+) or expressed as absolute number of Sytox Green-positive events per well. In addition, for some specific time points, representative images were presented to illustrate whether apoptotic or necroptotic cell death was engaged.

Immunofluorescence staining and analysis. *Mlkl*$^{-/-}$ MEF expressing DOX-inducible FLAG-MLKL (N-Term) were cultured in chamber slides (155382; Nunc Lab-Tek II). After treatment, cells were washed twice with PBS followed by fixation with 4% paraformaldehyde for 10 min at room temperature. Fixed cells were washed three times with TBS and permeabilized 3 min with 0.1% Triton-X-100 in TBS. Cells were blocked for 30 min with 2% BSA, 0.05% Tween-20 in TBS. Immunolabeling was performed at 4 °C overnight with primary antibodies (0.1 μg/ml of anti-pS345-MLKL, (clone 7C6.1) or 0.5 μg/ml of anti-FLAG). Then, cells were washed three times with 0.01% Tween-20 in TBS followed by incubation for 2 h at room temperature with fluorescently labeled secondary antibodies at a concentration of 0.5 μg/ml, and 0.1 μM fluorescently labeled phalloidin for F-actin labeling. Nuclei were stained using a final imaging buffer containing 1 μg/ml Hoechst in TBS. Plasma membrane localization of proteins was analyzed using an AxioObserver Z.1 inverted microscope equipped with 405 nm, 473 nm, 561 nm and 660 laser lines, CSU-22 spinning disc (Yokagawa), ×63 1.4 NA oil objective and EMCCD camera. To determine correlation of pMLKL with FLAG localization, images were acquired and analyzed using Slidebook software (Intelligent Imaging Innovations). In brief, the intensity values for each channel were determined on an individual pixel basis along a line drawn across an area of the cell, encompassing cytoplasm bounded by plasma membrane. The r^2 of intensity values was determined by Pearson's correlation function. All experiments were performed in at least three independent experiments.

Conflict of Interest

The authors declare no conflict of interest.

Acknowledgements. We thank William Zuercher from GlaxoSmithKline (GSK) for providing all compounds for RIPK3 inhibition. We also thank Mao Yang for technical assistance. This work was supported by grants from the U.S. National Institutes of Health and the American Lebanese Syrian Associated Charities.

1. Zhao J, Jitkaew S, Cai Z, Choksi S, Li Q, Luo J *et al.* Mixed lineage kinase domain-like is a key receptor interacting protein 3 downstream component of TNF-induced necrosis. *Proc Natl Acad Sci USA* 2012; **109**: 5322–5327.
2. Sun L, Wang H, Wang Z, He S, Chen S, Liao D *et al.* Mixed lineage kinase domain-like protein mediates necrosis signaling downstream of RIP3 kinase. *Cell* 2012; **148**: 213–227.
3. Murphy JM, Czabotar PE, Hildebrand JM, Lucet IS, Zhang JG, Alvarez-Diaz S *et al.* The pseudokinase MLKL mediates necroptosis via a molecular switch mechanism. *Immunity* 2013; **39**: 443–453.
4. Li J, McQuade T, Siemer AB, Napetschnig J, Moriwaki K, Hsiao YS *et al.* The RIP1/RIP3 necrosome forms a functional amyloid signaling complex required for programmed necrosis. *Cell* 2012; **150**: 339–350.
5. Green DR, Oberst A, Dillon CP, Weinlich R, Salvesen GS. RIPK-dependent necrosis and its regulation by caspases: a mystery in five acts. *Mol Cell* 2011; **44**: 9–16.
6. Weinlich R, Oberst A, Dillon CP, Janke LJ, Milasta S, Lukens JR *et al.* Protective roles for caspase-8 and cFLIP in adult homeostasis. *Cell Rep* 2013; **5**: 340–348.
7. Dillon CP, Oberst A, Weinlich R, Janke LJ, Kang TB, Ben-Moshe T *et al.* Survival function of the FADD-CASPASE-8-cFLIP(L) complex. *Cell Rep* 2012; **1**: 401–407.
8. Oberst A, Dillon CP, Weinlich R, McCormick LL, Fitzgerald P, Pop C *et al.* Catalytic activity of the caspase-8-FLIP(L) complex inhibits RIPK3-dependent necrosis. *Nature* 2011; **471**: 363–367.
9. Kaiser WJ, Upton JW, Long AB, Livingston-Rosanoff D, Daley-Bauer LP, Hakem R *et al.* RIP3 mediates the embryonic lethality of caspase-8-deficient mice. *Nature* 2011; **471**: 368–372.
10. Zhang H, Zhou X, McQuade T, Li J, Chan FK, Zhang J. Functional complementation between FADD and RIP1 in embryos and lymphocytes. *Nature* 2011; **471**: 373–376.
11. Dillon CP, Weinlich R, Rodriguez DA, Cripps JG, Quarato G, Gurung P *et al.* RIPK1 blocks early postnatal lethality mediated by caspase-8 and RIPK3. *Cell* 2014; **157**: 1189–1202.
12. Kaiser WJ, Daley-Bauer LP, Thapa RJ, Mandal P, Berger SB, Huang C *et al.* RIP1 suppresses innate immune necrotic as well as apoptotic cell death during mammalian parturition. *Proc Natl Acad Sci USA* 2014; **111**: 7753–7758.
13. Rickard JA, O'Donnell JA, Evans JM, Lalaoui N, Poh AR, Rogers T *et al.* RIPK1 regulates RIPK3-MLKL-driven systemic inflammation and emergency hematopoiesis. *Cell* 2014; **157**: 1175–1188.
14. Weinlich R, Green DR. The two faces of receptor interacting protein kinase-1. *Mol Cell* 2014; **56**: 469–480.
15. Chen X, Li W, Ren J, Huang D, He WT, Song Y *et al.* Translocation of mixed lineage kinase domain-like protein to plasma membrane leads to necrotic cell death. *Cell Res* 2014; **24**: 105–121.
16. Wang H, Sun L, Su L, Rizo J, Liu L, Wang LF *et al.* Mixed lineage kinase domain-like protein MLKL causes necrotic membrane disruption upon phosphorylation by RIP3. *Mol Cell* 2014; **54**: 133–146.
17. Cai Z, Jitkaew S, Zhao J, Chiang HC, Choksi S, Liu J *et al.* Plasma membrane translocation of trimerized MLKL protein is required for TNF-induced necroptosis. *Nat Cell Biol* 2014; **16**: 55–65.
18. Hildebrand JM, Tanzer MC, Lucet IS, Young SN, Spall SK, Sharma P *et al.* Activation of the pseudokinase MLKL unleashes the four-helix bundle domain to induce membrane localization and necroptotic cell death. *Proc Natl Acad Sci USA* 2014; **111**: 15072–15077.
19. Dondelinger Y, Declercq W, Montessuit S, Roelandt R, Goncalves A, Bruggeman I *et al.* MLKL compromises plasma membrane integrity by binding to phosphatidylinositol phosphates. *Cell Rep* 2014; **7**: 971–981.
20. Xie T, Peng W, Yan C, Wu J, Gong X, Shi Y. Structural insights into RIP3-mediated necroptotic signaling. *Cell Rep* 2013; **5**: 70–78.
21. Green DR. Pseudokiller, qu'est-ce que c'est? *Immunity* 2013; **39**: 421–422.
22. Weinert BT, Scholz C, Wagner SA, Iesmantavicius V, Su D, Daniel JA *et al.* Lysine succinylation is a frequently occurring modification in prokaryotes and eukaryotes and extensively overlaps with acetylation. *Cell Rep* 2013; **4**: 842–851.
23. Verdin E, Ott M. 50 years of protein acetylation: from gene regulation to epigenetics, metabolism and beyond. *Nat Rev Mol Cell Biol* 2014; **16**: 258–264.
24. Orozco S, Yatim N, Werner MR, Tran H, Gunja SY, Tait SW *et al.* RIPK1 both positively and negatively regulates RIPK3 oligomerization and necroptosis. *Cell Death Differ* 2014; **21**: 1511–1521.
25. Tait SW, Oberst A, Quarato G, Milasta S, Haller M, Wang R *et al.* Widespread mitochondrial depletion via mitophagy does not compromise necroptosis. *Cell Rep* 2013; **5**: 878–885.
26. Thapa RJ, Nogusa S, Chen P, Maki JL, Lerro A, Andrake M *et al.* Interferon-induced RIP1/RIP3-mediated necrosis requires PKR and is licensed by FADD and caspases. *Proc Natl Acad Sci USA* 2013; **110**: E3109–E3118.
27. Kaiser WJ, Sridharan H, Huang C, Mandal P, Upton JW, Gough PJ *et al.* Toll-like receptor 3-mediated necrosis via TRIF, RIP3, and MLKL. *J Biol Chem* 2013; **288**: 31268–31279.
28. Li JX, Feng JM, Wang Y, Li XH, Chen XX, Su Y *et al.* The B-Raf(V600E) inhibitor dabrafenib selectively inhibits RIP3 and alleviates acetaminophen-induced liver injury. *Cell Death Dis* 2014; **5**: e1278.
29. Wu XN, Yang ZH, Wang XK, Zhang Y, Wan H, Song Y *et al.* Distinct roles of RIP1-RIP3 hetero- and RIP3-RIP3 homo-interaction in mediating necroptosis. *Cell Death Differ* 2014; **21**: 1709–1720.
30. Chen W, Zhou Z, Li L, Zhong CQ, Zheng X, Wu X *et al.* Diverse sequence determinants control human and mouse receptor interacting protein 3 (RIP3) and mixed lineage kinase domain-like (MLKL) interaction in necroptotic signaling. *J Biol Chem* 2013; **288**: 16247–16261.
31. Dondelinger Y, Aguileta MA, Goossens V, Dubuisson C, Grootjans S, Dejardin E *et al.* RIPK3 contributes to TNFR1-mediated RIPK1 kinase-dependent apoptosis in conditions of cIAP1/2 depletion or TAK1 kinase inhibition. *Cell Death Differ* 2013; **20**: 1381–1392.
32. Tenev T, Bianchi K, Darding M, Broemer M, Langlais C, Wallberg F *et al.* The Ripoptosome, a signaling platform that assembles in response to genotoxic stress and loss of IAPs. *Mol Cell* 2011; **43**: 432–448.
33. Remijsen Q, Goossens V, Grootjans S, Van den Haute C, Vanlangenakker N, Dondelinger Y *et al.* Depletion of RIPK3 or MLKL blocks TNF-driven necroptosis and switches towards a delayed RIPK1 kinase-dependent apoptosis. *Cell Death Dis* 2014; **5**: e1004.
34. Mandal P, Berger SB, Pillay S, Moriwaki K, Huang C, Guo H *et al.* RIP3 induces apoptosis independent of pronecrotic kinase activity. *Mol Cell* 2014; **56**: 481–495.

35. Cook WD, Moujalled DM, Ralph TJ, Lock P, Young SN, Murphy JM *et al.* RIPK1- and RIPK3-induced cell death mode is determined by target availability. *Cell Death Differ* 2014; **21**: 1600–1612.
36. Roychowdhury S, McMullen MR, Pisano SG, Liu X, Nagy LE. Absence of receptor interacting protein kinase 3 prevents ethanol-induced liver injury. *Hepatology* 2013; **57**: 1773–1783.
37. Pereira FA, Mudgil AV, Rosmarin DM. Toxic epidermal necrolysis. *J Am Acad Dermatol* 2007; **56**: 181–200.
38. Kyung Kim S, Kim WJ, Yoon JH, Ji JH, Morgan MJ, Cho H *et al.* Upregulated RIP3 expression potentiates MLKL phosphorylation-mediated programmed necrosis in toxic epidermal necrolysis. *J Invest Dermatol* 2015; **135**: 2021–2030.
39. Vitner EB, Salomon R, Farfel-Becker T, Meshcheriakova A, Ali M, Klein AD *et al.* RIPK3 as a potential therapeutic target for Gaucher's disease. *Nat Med* 2014; **20**: 204–208.
40. Martinez J, Almendinger J, Oberst A, Ness R, Dillon CP, Fitzgerald P *et al.* Microtubule-associated protein 1 light chain 3 alpha (LC3)-associated phagocytosis is required for the efficient clearance of dead cells. *Proc Natl Acad Sci USA* 2011; **108**: 17396–17401.

Supplementary Information accompanies this paper on Cell Death and Differentiation website (http://www.nature.com/cdd)